Research Square

Preprints are preliminary reports that have not undergone peer review.
They should not be considered conclusive, used to inform clinical practice,
or referenced by the media as validated information.

Late Time Weak Field Scaling Consistency Test for the Hubble and S8 Cosmological Tensions

Andrew Morton

mortonam@iu.edu

Indiana University

Research Article

Keywords: ΛCDM consistency, cosmological tensions, Hubble tension, weak lensing, strong lensing time delays, public likelihood products

Posted Date: March 18th, 2026

DOI: https://doi.org/10.21203/rs.3.rs-8928023/v1

License: This work is licensed under a Creative Commons Attribution 4.0 International License. Read Full License

Additional Declarations: No competing interests reported.

Late Time Weak Field Scaling Consistency Test for the Hubble and S8 Cosmological Tensions

Andrew Morton[1*]

[1*]Independent Researcher.

Corresponding author(s). E-mail(s): mortonam@iu.edu;

Abstract

High-precision cosmological probes show persistent, probe-dependent shifts in inferred late-time parameters, notably (i) the difference between early-time (CMB-inferred) and late-time determinations of the Hubble constant H_0, and (ii) the lower late-time clustering amplitude inferred from weak lensing, often summarized by $S_8 \equiv \sigma_8\sqrt{\Omega_m/0.3}$. We present a deliberately minimal and falsifiable consistency diagnostic for **ΛCDM** rather than a complete modified-gravity theory: we introduce a single phenomenological parameter s that rescales the effective weak-field amplitude relevant for time delays and lensing, activated only below a fixed redshift gate z_* (fiducial value $z_* = 0.7$). Under a conservative observable-level mapping (no scale dependence, no gravitational slip, and no modification to the background expansion), the same s maps onto strong-lens time-delay distance likelihoods and (approximately) onto the cosmic-shear amplitude direction. Using publicly released time-delay distance likelihood products from strong-lens cosmography and the publicly released KiDS-1000 cosmic shear posterior, we obtain $s_{\rm lens} = 0.9156^{+0.0245}_{-0.0212}$ and $s_{\rm WL} = 0.9023^{+0.0280}_{-0.0303}$ (68% credible intervals), with posterior overlap $\mathcal{O} = 0.7626$ and a descriptive difference-of-means proxy $T = 0.4297\sigma$. Rather than proposing a new cosmological model, this work introduces a one-parameter weak-field scaling diagnostic that can be applied directly to existing late-time observational data. The full analysis is reproducible with an open notebook that downloads the public products and records provenance including repository commit identifiers and SHA-256 hashes.

Keywords: **ΛCDM** consistency, cosmological tensions, Hubble tension, weak lensing, strong lensing time delays, public likelihood products

1 Introduction

1.1 Late-time discrepancies and cross-probe closure

The ΛCDM cosmological model provides an excellent description of a wide range of observations, including the cosmic microwave background (CMB), within a compact parameter space [1]. As observational precision has improved, however, comparisons among late-time probes have revealed persistent, probe-dependent shifts in inferred cosmological parameters that are not trivially accommodated within baseline ΛCDM [2, 3].

Two prominent examples are the Hubble tension and the S_8 tension. The Hubble tension refers to the discrepancy between the value of H_0 inferred from early-universe CMB data under ΛCDM [1] and that measured using low-redshift probes, including distance-ladder observations [4], strong-lens time-delay cosmography [5], and standard sirens [6]. The S_8 tension arises from weak-lensing surveys that prefer a lower clustering amplitude than the CMB-inferred ΛCDM value [7, 8]. The origin of these discrepancies remains unsettled, with proposed explanations spanning unaccounted-for systematics, statistical fluctuations, and extensions to the standard cosmological framework [2, 3].

A natural question is whether multiple late-time discrepancies can be coherently characterized by a common phenomenological modification at the level of observables. This motivates a closure diagnostic: can two independent weak-field probes be brought into mutual statistical consistency by the same minimal deformation of their late-time inference mapping?

1.2 A one-parameter late-time scaling diagnostic

We introduce a single-parameter diagnostic defined by an effective late-time scaling factor s that rescales weak-field observables below a fixed redshift threshold z_*. Operationally, s is defined through its action on released likelihood and posterior products. It modifies the observables entering (i) time-delay strong-lens cosmography and (ii) cosmic-shear amplitude measurements in a controlled, multiplicative manner (Sec. 3).

If a dominant contribution to the observed late-time discrepancies can be represented as a single multiplicative distortion of weak-field observables, then independent probes should infer statistically compatible posteriors for s. A significant mismatch between these posteriors disfavors the broad class of single-factor late-time explanations and instead points toward probe-specific systematics or more structured extensions that cannot be reduced to an amplitude-only rescaling.

This construction is intended as a consistency test rather than a full likelihood-level reanalysis of survey data. The primary result is the degree of agreement between independently inferred s posteriors. For orientation, we also translate any mutually preferred s into implied shifts in H_0 and S_8 using the mappings defined in Sec. 3.

1.3 Notation: S_8 versus s

We reserve S_8 for the conventional cosmic-shear amplitude parameter,

$$S_8 \equiv \sigma_8 \sqrt{\Omega_m/0.3}.$$

The symbol s denotes the effective late-time scaling parameter introduced here. Because s is defined through its action on weak-field observables below z_*, it is not assumed to coincide with a locally measured Newton constant in screened or high-density environments.

1.4 Data products, analysis outline, and reproducibility

We infer s independently from two publicly available data products. For strong-lens time-delay cosmography, we use released time-delay distance likelihood products [5, 9] to construct $p_{\rm lens}(s)$. For weak-lensing cosmic shear, we use public KiDS-1000 posterior samples [7, 10] to construct $p_{\rm WL}(s)$ under the same mapping. We quantify agreement between the resulting posteriors using an overlap-based consistency metric (Sec. 5.3) and translate any mutually preferred s into implied shifts in H_0 and S_8.

All results are reproducible via a companion notebook [11] that performs the analysis end-to-end from public inputs, regenerates all figures and tables, and exports a provenance record including data URLs, file hashes, software versions, and commit identifiers where applicable.

2 Diagnostic parameterization: a one-parameter late-time scaling

2.1 Gate definition

We introduce a late-time scaling parameter s that is activated only below a fixed redshift threshold z_*:

$$s(z) = \begin{cases} 1, & z \geq z_*, \\ s, & z < z_*, \end{cases} \tag{1}$$

with fiducial value $z_* = 0.7$. Throughout the main analysis z_* is held fixed; alternative values are explored as robustness tests. This construction ensures that early-time observables, including recombination-era physics, remain unchanged by definition.

2.2 Controlled observable-level mapping

The diagnostic is intentionally defined at the level of observables rather than as a full modification of the cosmological field equations. Specifically, we adopt the following controlled assumptions: the background expansion history and distance–redshift relation are fixed to a reference ΛCDM cosmology; the scaling parameter s is taken to be constant within the late-time window $z < z_*$, with no scale dependence; and the two gravitational potentials relevant for lensing and non-relativistic dynamics are assumed to scale identically, such that no gravitational slip is introduced.

These restrictions isolate a minimal amplitude-like deformation of weak-field observables. The purpose is to test whether a single multiplicative late-time distortion can provide cross-probe statistical closure. Failure of closure under this restricted deformation disfavors the class of single-factor amplitude explanations, while agreement would motivate a more detailed likelihood-level investigation.

3 Observable-level mapping

3.1 Strong-lens time-delay distances

In time-delay strong-lens cosmography, the time delay between two images A, B is

$$\Delta t_{AB} = \frac{D_{\Delta t}}{c}\,\Delta\phi_{AB}, \tag{2}$$

where $\Delta\phi_{AB}$ is the Fermat-potential difference determined by lens modeling and

$$D_{\Delta t} \equiv (1+z_L)\frac{D_L D_S}{D_{LS}} \tag{3}$$

is the time-delay distance, with D denoting angular-diameter distances.

3.1.1 Definition of s

For lenses with $z_L < z_*$, we define the phenomenological mapping

$$D_{\Delta t}^{\rm model}(s) = \begin{cases} s\, D_{\Delta t}^{\rm baseline}, & z_L < z_*, \\ D_{\Delta t}^{\rm baseline}, & z_L \geq z_*, \end{cases} \tag{4}$$

where $D_{\Delta t}^{\rm baseline}$ is evaluated in a fixed reference ΛCDM cosmology. Equation (4) defines s operationally for the lensing component of the diagnostic.

For fixed dimensionless distance ratios, $D_{\Delta t} \propto H_0^{-1}$, implying

$$H_0^{\rm implied} \approx \frac{H_0^{\rm baseline}}{s}. \tag{5}$$

Equation (5) is used only to translate s into an equivalent shift in H_0 for interpretive purposes; the primary inference is performed directly on s.

Scope of the reinterpretation.

Published $D_{\Delta t}$ likelihood products are derived under GR-based lens modeling assumptions. The transformation in Eq. (4) therefore constitutes a reparameterization of the released likelihood surface rather than a self-consistent reanalysis of imaging and stellar kinematics. This diagnostic is intended to assess posterior compatibility under a minimal multiplicative deformation; limitations of this approximation are discussed in Sec. 7.

3.2 Weak lensing and S_8

Weak gravitational lensing probes projected fluctuations in the lensing potential. Under the no-slip assumption introduced in Sec. 2, a late-time multiplicative rescaling of the potential amplitude yields

$$\kappa \to s\,\kappa_0, \qquad \gamma \to s\,\gamma_0,$$

so that two-point shear statistics scale approximately as

$$\xi_{\pm} \to s^2\, \xi_{\pm,0}. \tag{6}$$

Cosmic-shear posteriors are well described, to leading order, by the amplitude parameter

$$S_8 \equiv \sigma_8 \sqrt{\Omega_m/0.3}.$$

To construct a diagnostic mapping consistent with the observable-level scaling above, we adopt the approximation

$$S_8^{\rm WL} \approx s\, S_8^{\rm baseline} \qquad \Longleftrightarrow \qquad s \approx \frac{S_8^{\rm WL}}{S_8^{\rm baseline}}. \tag{7}$$

Equation (7) does not replace a full likelihood-level modification, which would require recomputation of growth and lensing kernels within a modified theory. Instead, it provides a transparent mapping from the released S_8 posterior to an effective s posterior suitable for the closure test.

Kernel support and gate interpretation.

Cosmic-shear kernels span a broad redshift range. In this first-pass diagnostic, the s inferred from S_8 is interpreted as an effective kernel-averaged scaling parameter over the survey redshift distribution, rather than a piecewise evaluation of Eq. (1) within the shear kernel itself.

4 Data

4.1 Baseline reference cosmology

All baseline distances entering the lens mapping are evaluated in a spatially flat ΛCDM cosmology consistent with Planck 2018 constraints [1]. We adopt

$$H_0^{\rm baseline} = 67.36\,{\rm km\,s^{-1}\,Mpc^{-1}}, \qquad \Omega_{\rm m}^{\rm baseline} = 0.3153.$$

For translating s into an equivalent shift in the shear-amplitude parameter, we use

$$S_8^{\rm baseline} = 0.8320.$$

The baseline cosmology is held fixed throughout; s acts only through the observable-level mappings defined in Sec. 3.

4.2 Strong-lens time-delay likelihood products

We use publicly released time-delay distance likelihood products from the H0LiCOW/TDCOSMO analyses [5, 9] for the following systems:

Lens	z_L	z_S
RXJ1131−1231	0.295	0.654
PG1115+080	0.311	1.722
HE0435−1223	0.4546	1.693
B1608+656	0.6304	1.394
WFI2033−4723	0.6575	1.662
SDSS J1206+4332	0.745	1.789

For the fiducial gate $z_* = 0.7$, all systems except SDSS J1206+4332 satisfy $z_L < z_*$ and therefore enter the late-time window under Eq. (1). The released likelihood surfaces are used directly in the reparameterized form described in Sec. 3.

4.3 KiDS-1000 weak-lensing posterior samples

For cosmic shear, we use publicly released KiDS-1000 posterior samples [7, 10]. From the public posterior sample file we extract the derived parameter S_8. For the dataset analyzed here, the posterior summary is

$$S_8^{\rm KiDS} = 0.7495 \pm 0.0219,$$

where uncertainties denote the standard deviation of the sampled posterior. The full chain is used to construct the effective $p_{\rm WL}(s)$ posterior under Eq. (7).

4.4 Reproducibility and provenance

All inputs are obtained from publicly available repositories. The companion notebook records machine-readable provenance metadata, including repository URLs, commit identifiers, file hashes, and software versions.

A complete provenance record (JSON format) accompanies the analysis and contains the exact commit hash of the H0LiCOW repository and the SHA-256 digest of the KiDS-1000 archive used in this work.

5 Method

5.1 Inference of s from strong lenses

Let $\mathcal{L}_i(D_{\Delta t})$ denote the released likelihood surface (or published likelihood surrogate) for lens i as a function of the time-delay distance $D_{\Delta t}$.

For a fixed baseline cosmology, we compute $D_{\Delta t,i}^{\rm baseline}$ from the measured (z_L, z_S) of each system. The gate-modified model prediction $D_{\Delta t,i}^{\rm model}(s)$ is defined by Eq. (4).

Assuming statistical independence among lens systems, the joint likelihood is

$$\log \mathcal{L}_{\rm lens}(s) = \sum_i \log \mathcal{L}_i\big(D_{\Delta t,i}^{\rm model}(s)\big)\,. \tag{8}$$

We adopt a uniform prior $\pi(s)$ over $s \in [0.8, 1.2]$, implemented on a fixed grid (801 points). The posterior is then

$$p_{\rm lens}(s) \propto \pi(s)\, \mathcal{L}_{\rm lens}(s), \tag{9}$$

with normalization performed numerically over the s grid. The posterior support lies well within this prior range for the present run, so edge effects are negligible.

The released likelihood products are used directly without re-fitting imaging or stellar kinematics. The resulting $p_{\rm lens}(s)$ should therefore be interpreted as a reparameterization of the published likelihood surfaces under the mapping of Sec. 3.

5.2 Inference of s from weak lensing

Using the amplitude-level mapping in Eq. (7), we transform the KiDS posterior samples from S_8 into an effective posterior for s. To propagate the quoted Planck uncertainty in $S_8^{\rm baseline}$, we draw Monte Carlo samples $S_8^{\rm baseline} \sim \mathcal{N}(0.8320, 0.013)$ and resample $S_8^{\rm WL}$ from the weighted KiDS posterior sample file. For each paired draw we compute

$$s = \frac{S_8^{\rm WL}}{S_8^{\rm baseline}}. \tag{10}$$

The resulting Monte Carlo ensemble defines $p_{\rm WL}(s)$. For the overlap integral and the mean/variance proxy we restrict the density estimate to the common grid range $s \in [0.8, 1.2]$ used for the lens posterior; this matches the notebook implementation and avoids KDE tails outside the evaluated support. To compare with the lens posterior, we evaluate both densities on a common s grid. For visualization and overlap evaluation we use a Gaussian kernel density estimate (SciPy `gaussian_kde` with default bandwidth) evaluated on the same grid as the lens posterior.

5.3 Consistency metrics

The primary objective is to assess posterior compatibility between $p_{\rm lens}(s)$ and $p_{\rm WL}(s)$.

We quantify agreement using two complementary descriptive statistics.

Posterior overlap.

We compute the normalized overlap

$$\mathcal{O} = \int ds\ \min[p_{\rm lens}(s),\, p_{\rm WL}(s)]\,, \tag{11}$$

where $0 \leq \mathcal{O} \leq 1$. Identical posteriors yield $\mathcal{O} = 1$, while non-overlapping posteriors yield $\mathcal{O} = 0$.

Difference-of-means statistic.

As a complementary summary, we report

$$T = \frac{|\mu_{\rm lens} - \mu_{\rm WL}|}{\sqrt{\sigma^2_{\rm lens} + \sigma^2_{\rm WL}}}, \tag{12}$$

where μ and σ denote posterior mean and standard deviation, respectively. The quantity T is quoted as an effective Gaussian-equivalent separation. It is a descriptive measure of offset and is not interpreted as a Bayesian evidence ratio.

5.4 Robustness checks

This first-pass notebook includes two targeted checks: (i) recomputation of $p_{\rm lens}(s)$ for a small set of fixed gate values z_* (Table 2), and (ii) weak-lensing parsing safeguards (explicit MultiNest weight inference and hard-fail behavior if S_8 cannot be extracted from the public chain).

Additional robustness analyses (e.g., leave-one-out lens tests and explicit prior-range sweeps) are straightforward extensions but are not included in the present draft.

6 Results

6.1 Posterior inference and cross-probe closure

For the fiducial gate $z_* = 0.7$, we obtain

$$s_{\rm lens} = 0.9156^{+0.0245}_{-0.0212} \qquad (68\%\ \mathrm{CI}:\ [0.8944,\ 0.9400]), \tag{13}$$

$$s_{\rm WL} = 0.9023^{+0.0280}_{-0.0303} \qquad (68\%\ \mathrm{CI}:\ [0.8720,\ 0.9303]). \tag{14}$$

The resulting posteriors overlap at the level

$$\mathcal{O} = 0.7626, \qquad T = 0.4297\sigma,$$

according to the consistency metrics defined in Sec. 5.3. Within this diagnostic construction, the two probes therefore yield statistically compatible estimates of s.

6.2 Translation to implied H_0 and S_8

Using Eq. (5) with $H_0^{\rm baseline} = 67.36\,\mathrm{km\,s^{-1}\,Mpc^{-1}}$, the strong-lens posterior corresponds to an implied value

$$H_0^{\rm implied} = 73.6\,\mathrm{km\,s^{-1}\,Mpc^{-1}} \quad (68\%\ \mathrm{CI}:\ [71.7\,\mathrm{km\,s^{-1}\,Mpc^{-1}},\ 75.3\,\mathrm{km\,s^{-1}\,Mpc^{-1}}]). \tag{15}$$

Under the single-factor hypothesis, the same $s_{\rm lens}$ predicts

$$S_8^{\rm implied} = s_{\rm lens}\, S_8^{\rm baseline} \approx 0.7617 \quad (68\%\ \mathrm{CI}:\ [0.7441,\ 0.7821]). \tag{16}$$

This predicted amplitude is consistent with the KiDS-1000 posterior summary $S_8^{\rm KiDS} = 0.7495 \pm 0.0219$ within the uncertainty range of the diagnostic mapping.

6.3 Summary table

Table 1 collects the inferred scaling parameter and the corresponding implied translations under the mappings of Sec. 3.

Table 1 Inferred scaling parameter s from strong-lens time-delay likelihood products and KiDS-1000 cosmic shear. The $H_0^{\rm implied}$ column uses Eq. (5) with $H_0^{\rm baseline} = 67.36\,{\rm km\,s^{-1}\,Mpc^{-1}}$. The $S_8^{\rm implied}$ column uses $S_8^{\rm baseline} = 0.8320$.

Probe	s (median, 68% CI)	$H_0^{\rm implied}$ [km s^{-1} Mpc^{-1}]	$S_8^{\rm implied}$
Strong lenses	0.9156 [0.8944, 0.9400]	73.6 [71.7, 75.3]	0.7617 [0.7441, 0.7821]
KiDS-1000 cosmic shear	0.9023 [0.8720, 0.9303]	···	0.7495 ± 0.0219

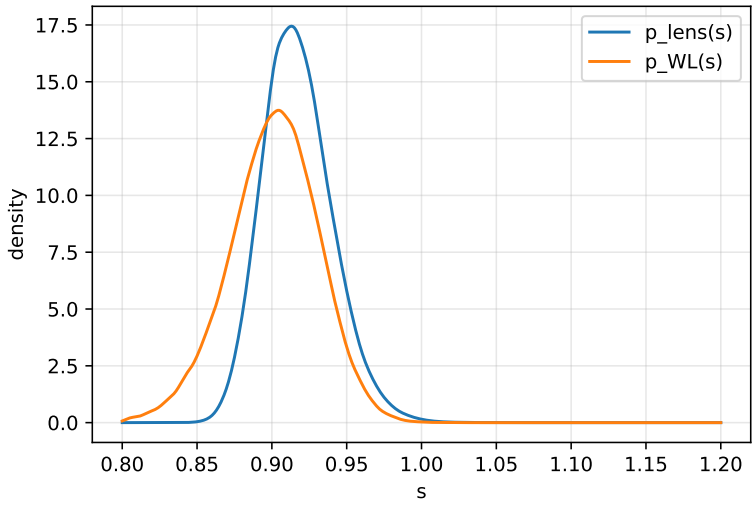


Fig. 1 Posterior densities $p_{\rm lens}(s)$ and $p_{\rm WL}(s)$ for the fiducial gate $z_* = 0.7$. The figure is generated directly by the companion notebook to ensure numerical consistency between the manuscript and the analysis output.

6.4 Posterior comparison

7 Robustness and limitations

7.1 Gate sensitivity

The step-function gate defined in Eq. (1) is a deliberate idealization. To assess sensitivity to this choice, we repeat the strong-lens inference for fixed alternative values of z_*. The results are summarized in Table 2.

Across these representative gate choices, the inferred s shifts smoothly as lenses enter or leave the gated subset, indicating that the fiducial result is not sharply tuned to the specific choice $z_* = 0.7$.

Table 2 Dependence of the strong-lens inference on the choice of gate redshift z_*.

Gate z_*	Lenses gated (of 6)	$s_{\rm lens}$ (median, 68% CI)
0.5	3	0.8788 [0.8508, 0.9107]
0.7	5	0.9156 [0.8944, 0.9400]
0.9	6	0.9175 [0.8971, 0.9404]

7.2 Use of released likelihood and posterior products

Both the strong-lens and weak-lensing inputs are publicly released likelihood or posterior products constructed under standard assumptions, including General Relativity, specific lens mass modeling choices, and survey-level nuisance parameter treatments. The reinterpretation under $s \neq 1$ therefore constitutes a reparameterization of these released products rather than a full forward-model likelihood reanalysis.

A complete treatment would require re-evaluating lens mass models and stellar kinematics under the modified mapping to determine whether the published $D_{\Delta t}$ likelihoods remain sufficient summaries of the imaging and dynamical information. Similarly, a self-consistent weak-lensing analysis would require implementing the modification within a full cosmic shear likelihood, including altered growth, lensing kernels, intrinsic alignment modeling, and baryonic feedback prescriptions.

The present construction is intended as a controlled diagnostic: it tests posterior compatibility under a minimal multiplicative deformation, without claiming self-consistency at the field-equation level.

7.3 Falsifiability of the single-factor hypothesis

Within this framework, the single-factor late-time closure hypothesis is disfavored if the independently inferred posteriors $p_{\rm lens}(s)$ and $p_{\rm WL}(s)$ exhibit negligible overlap under conservative prior choices, or if the degree of overlap is unstable under prespecified robustness tests (in this draft we report only gate variations; lens subsample exclusions and explicit prior-range sweeps are left for future work).

Conversely, sustained posterior compatibility under these checks would motivate a likelihood-level investigation of structured late-time modifications, but would not by itself establish a specific underlying theory.

8 Discussion

8.1 Interpretation of the one-parameter diagnostic

The construction presented here is intentionally minimal. It reparameterizes released likelihood and posterior products using a single late-time amplitude-like deformation. While this does not constitute a complete modified-gravity model, it serves a distinct purpose: to test whether independent weak-field probes can be brought into statistical consistency under a common multiplicative mapping.

Many proposed resolutions of late-time tensions introduce additional degrees of freedom, often with complex scale or redshift dependence. Before exploring higher-dimensional model spaces, it is informative to determine whether a single effective parameter is sufficient to reconcile the dominant discrepancies at the observable level. A positive result indicates structural compatibility across probes; a negative result disfavors the broad class of single-factor amplitude explanations.

8.2 Late-time scope and interpretation limits

By construction, the diagnostic acts only at low redshift. The background expansion history and recombination-era physics remain fixed to the reference ΛCDM cosmology. Consequently, the analysis does not address early-time extensions, recombination physics, or tensions that arise primarily in the high-redshift regime.

The implied shifts in H_0 and S_8 reported in Sec. 6 should therefore be interpreted conditionally, within the observable-level mapping of Sec. 3, rather than as evidence for a specific underlying theory.

8.3 Path toward likelihood-level tests

If cross-probe compatibility persists under robustness checks, a natural extension would be a likelihood-level implementation of the same deformation. Such an analysis would require: (i) revisiting strong-lens imaging and stellar kinematics within the modified mapping, (ii) implementing the deformation in a full cosmic-shear likelihood including growth evolution, lensing kernels, intrinsic alignments, and baryonic feedback, and (iii) incorporating additional late-time probes such as supernova distances, BAO measurements, and standard sirens to overconstrain the parameter space.

The present results provide a quantitative basis for determining whether such an extended program is warranted.

9 Conclusion

We presented a one-parameter, late-time weak-field scaling diagnostic designed to test whether a single multiplicative factor s can jointly account for both the H_0 and S_8 tensions in a cross-probe closure sense. The key feature is overconstraint: time-delay strong lenses and weak-lensing cosmic shear must infer the same s for the explanation to remain viable. Using public time-delay distance likelihood products and the public KiDS-1000 cosmic shear posterior, we find consistent s posteriors with statistically compatible overlap. The analysis is implemented in an open notebook that automatically downloads public data products and reproduces all results. Future work should upgrade the diagnostic mapping used here to a likelihood-level implementation if, and only if, the cross-probe consistency test motivates it.

The author acknowledges the use of large language models for assistance in symbolic computation, LaTeX formatting, and mathematical formalism throughout the development of this work. We thank the open-source and academic communities for the availability of foundational tools and literature that make independent theoretical work of this nature possible.

Declarations

Consent to Publish

Consent to Publish declaration: not applicable.

Consent to Participate

Consent to Participate declaration: not applicable.

Ethics Approval

Ethics declaration: not applicable.

Clinical Trial Registration

This study is not a clinical trial. Registration details are not applicable.

Funding

The author received no specific funding for this work.

Competing interests

The author declares no competing interests.

Data availability

The datasets analyzed in this study are publicly available from the Planck, SH0ES, and DES collaborations. Derived analysis products and scripts used in this work are available in the Zenodo repository at https://doi.org/10.5281/zenodo.18712291.

Code availability

The analysis notebook used to generate the results and figures in this manuscript is available in the Zenodo record associated with this work (DOI: 10.5281/zenodo.18712291) and is designed to reproduce the full pipeline from raw public products.

Appendix A Reproducibility and data provenance

The companion notebook exports a machine-readable provenance record (JSON format) containing, for each public data product used in this analysis:

- Source URL,
- Filename,
- SHA-256 checksum,
- Access date,
- Repository commit identifier (where applicable),
- Software environment metadata.

This provenance file accompanies the reproducible analysis pipeline and can be provided as supplementary material to ensure exact numerical replication.

References

[1] Planck Collaboration, Aghanim, N., Akrami, Y., Ashdown, M., *et al.*: Planck 2018 results. vi. cosmological parameters. Astronomy & Astrophysics **641**, 6 (2020) https://doi.org/10.1051/0004-6361/201833910 arXiv:1807.06209 [astro-ph.CO]

[2] Verde, L., Treu, T., Riess, A.G.: Tensions between the early and late universe. Nature Astronomy **3**, 891–895 (2019) https://doi.org/10.1038/s41550-019-0902-0 arXiv:1907.10625 [astro-ph.CO]

[3] Abdalla, E., Abellán, G.F., Aboubrahim, A., *et al.*: Cosmology intertwined: A review of the particle physics, astrophysics, and cosmology associated with the cosmological tensions and anomalies. Journal of High Energy Astrophysics **34**, 49–211 (2022) https://doi.org/10.1016/j.jheap.2022.04.002 arXiv:2203.06142 [astro-ph.CO]

[4] Riess, A.G., Yuan, W., Macri, L.M., Scolnic, D., Brout, D., *et al.*: A comprehensive measurement of the local value of the hubble constant with 1 km s^{-1} mpc^{-1} uncertainty from the hubble space telescope and the sh0es team. The Astrophysical Journal Letters **934**, 7 (2022) https://doi.org/10.3847/2041-8213/ac5c5b arXiv:2112.04510 [astro-ph.CO]

[5] Wong, K.C., Suyu, S.H., Chen, G.C.-F., Rusu, C.E., Millon, M., Sluse, D., *et al.*: H0LiCOW – xiii. a 2.4 per cent measurement of H_0 from lensed quasars: 5.3σ tension between early- and late-universe probes. Monthly Notices of the Royal Astronomical Society **498**(1), 1420–1439 (2020) https://doi.org/10.1093/mnras/stz3094 arXiv:1907.04869 [astro-ph.CO]

[6] Abbott, B.P., *et al.*: A gravitational-wave standard siren measurement of the hubble constant. Nature **551**(7678), 85–88 (2017) https://doi.org/10.1038/nature24471 arXiv:1710.05835 [astro-ph.CO]

[7] Asgari, M., Lin, C.-A., Joachimi, B., Giblin, B., Heymans, C., Hildebrandt, H., *et al.*: KiDS-1000 cosmology: Cosmic shear constraints and comparison between two point statistics. Astronomy & Astrophysics **645**, 104 (2021) https://doi.org/10.1051/0004-6361/202039070 arXiv:2007.15633 [astro-ph.CO]

[8] Amon, A., Gruen, D., Troxel, M.A., MacCrann, N., Dodelson, S., Choi, A., Doux, C., Secco, L.F., Samuroff, S., Krause, E., *et al.*: Dark energy survey year 3 results: Cosmology from cosmic shear and robustness to data calibration. Physical Review D **105**(2), 023514 (2022) https://doi.org/10.1103/PhysRevD.105.023514 arXiv:2105.13543 [astro-ph.CO]

[9] Birrer, S., Shajib, A.J., Galan, A., Millon, M., Treu, T., Agnello, A., Auger, M., *et al.*: TDCOSMO. iv. hierarchical time-delay cosmography – joint inference of the hubble constant and galaxy density profiles. Astronomy & Astrophysics **643**, 165 (2020) https://doi.org/10.1051/0004-6361/202038861 arXiv:2007.02941 [astro-ph.CO]

[10] Heymans, C., Tröster, T., Asgari, M., Blake, C., Hildebrandt, H., Joachimi, B., Kuijken, K., *et al.*: KiDS-1000 cosmology: Multi-probe weak gravitational lensing and spectroscopic galaxy clustering constraints. Astronomy & Astrophysics **646**, 140 (2021) https://doi.org/10.1051/0004-6361/202039063 arXiv:2007.15632 [astro-ph.CO]

[11] Morton, A.: A One-Parameter Late-Time Weak-Field Scaling Consistency Test for the H_0 and S_8 Tensions. Zenodo. Zenodo record (includes associated Colab code and reproducibility bundle). (2026). https://doi.org/10.5281/zenodo.18712291